The Astrophysical Journal, 869:110 (7pp), 2018 December 20 https://doi.org/10.3847/1538-4357/aaec7b

Propagating Spectropolarimetric Disturbances in a Large Sunspot

M. Stangalini[1], S. Jafarzadeh[2,3], I. Ermolli[1], R. Erdélyi[4,5], D. B. Jess[6,7], P. H. Keys[6], F. Giorgi[1], M. Murabito[1], F. Berrilli[8], and D. Del Moro[8]
[1] INAF-OAR National Institute for Astrophysics, Via Frascati 33, I-00078 Monte Porzio Catone (RM), Italy; marco.stangalini@inaf.it
[2] Rosseland Centre for Solar Physics, University of Oslo, P.O. Box 1029 Blindern, NO-0315 Oslo, Norway
[3] Institute of Theoretical Astrophysics, University of Oslo, P.O. Box 1029 Blindern, NO-0315 Oslo, Norway
[4] Solar Physics & Space Plasma Research Centre (SP2RC), School of Mathematics and Statistics, University of Sheffield, Sheffield S3 7RH, UK
[5] Department of Astronomy, Eötvös L. University, Pázmány P. sétány 1/A, Budapest H-1117, Hungary
[6] Astrophysics Research Centre, School of Mathematics and Physics, Queen's University Belfast, Belfast BT7 1NN, UK
[7] Department of Physics and Astronomy, California State University Northridge, Northridge, CA 91330, USA
[8] Department of Physics, Università di Roma Tor Vergata, Via della Ricerca Scientifica 1, I-00133, Rome, Italy
Received 2018 May 3; revised 2018 October 25; accepted 2018 October 25; published 2018 December 17

Abstract

We present results derived from the analysis of spectropolarimetric measurements of active region AR12546, which represents one of the largest sunspots to have emerged onto the solar surface over the last 20 years. The region was observed with full-Stokes scans of the Fe I 617.3 nm and Ca II 854.2 nm lines with the Interferometric BIdimensional Spectrometer instrument at the Dunn Solar Telescope over an uncommon, extremely long time interval exceeding three hours. Clear circular polarization (CP) oscillations localized at the umbra–penumbra boundary of the observed region were detected. Furthermore, the multi-height data allowed us to detect the downward propagation of both CP and intensity disturbances at 2.5–3 mHz, which was identified by a phase delay between these two quantities. These results are interpreted as a propagating magnetohydrodynamic surface mode in the observed sunspot.

Key words: polarization – Sun: chromosphere – Sun: magnetic fields – Sun: oscillations – Sun: photosphere – sunspots

1. Introduction

Driven by the forcing action of steady and impulsive photospheric plasma motion, a large variety of magnetohydrodynamic (MHD) modes (e.g., kink, torsional Alfvén, sausage) can be excited in sunspots and small-scale magnetic field concentrations (e.g., Edwin & Roberts 1983; Roberts 1983; Khomenko et al. 2008; Felipe et al. 2010; Fedun et al. 2011; Mumford & Erdélyi 2015; Mumford et al. 2015; Löhner-Böttcher 2016; Grant et al. 2018; Keys et al. 2018). In addition, the magnetic field concentrations can interact with the surrounding *p*- and *f*-mode oscillations, and these can be eventually absorbed and converted into magneto-acoustic waves that can propagate along the field guide to the upper layers of the solar atmosphere (see for example Braun et al. 1992; Cally et al. 1994; Crouch & Cally 2005; Moretti et al. 2007; Vigeesh et al. 2012; Freij et al. 2014; Grant et al. 2015; Jess et al. 2017; Pintér & Erdélyi 2018). There is a general consensus that MHD waves can play a significant role in the energy budget of the solar atmosphere (Jess et al. 2009, 2015; Felipe et al. 2011; Morton et al. 2012; Mathioudakis et al. 2013; Krishna Prasad et al. 2017).

From an observational point of view, a wealth of wave signatures in different observables have been reported so far at different heights in the solar atmosphere and in different kinds of magnetic structures, based on intensity and Doppler velocity measurements (Bogdan 2000; Centeno et al. 2006; Chorley et al. 2010; Morton et al. 2011; Stangalini et al. 2012; Grant et al. 2015; Jafarzadeh et al. 2017; Jess et al. 2017). The propagation of these disturbances depends on the local physical parameters and the geometry of the waveguide (Jefferies et al. 2006; McIntosh & Jefferies 2006; Bloomfield et al. 2007; Stangalini et al. 2011; Moreels et al. 2015; Allcock & Erdélyi 2017; Zsámberger et al. 2018).

In addition to intensity and Doppler velocity oscillations, magnetic field perturbations are also expected in the case of particular MHD modes (Edwin & Roberts 1983; Roberts 1983). Several attempts have been made to detect such oscillations in different magnetic structures in the Sun's atmosphere. Many authors have reported magnetic field oscillations with periods in the range 3–5 min and amplitudes of the order of 10 G (e.g., Horn et al. 1997; Balthasar 1999; Rüedi et al. 1999; Bellot Rubio et al. 2000; Staude 2002; Houston et al. 2018). However, based on the available observations, the unambiguous attribution of these perturbations to magnetic oscillations has been debated (Staude 2002).

Indeed, by making use of spectropolarimetric inversions in the photosphere, Lites et al. (1998) found an upper limit for the amplitude of the magnetic fluctuations in a large symmetric sunspot located near the disk center of the order of 4 G, and interpreted them to be of instrumental origin. Independent studies also found that significant magnetic oscillations are inhomogeneously distributed and concentrated in patches (Rueedi et al. 1998), or at the umbra–penumbra boundary in sunspots (Balthasar 1999; Kupke et al. 2000). Through phase lag analyses between different physical quantities, it was shown that these magnetic perturbations were not consistent with cross-talk between either the Doppler shift of the line, or the intensity. Based on this, Kupke et al. (2000) argued that the observed oscillations of the Stokes parameters in sunspots could be interpreted as real magnetic field perturbations resulting from the swaying of the field lines in response to the driving action of *p*-modes.

Fujimura & Tsuneta (2009), using spectropolarimetric data of the solar photosphere acquired by *Hinode* SOT/SP (Tsuneta

et al. 2008), reported the presence of magnetic flux oscillations in pores and other magnetic concentrations and interpreted them as the signature of sausage and kink modes. More recently, Martínez González et al. (2011), by taking advantage of the unprecedented high spatial resolution achieved by the balloon-borne SUNRISE mission (Solanki et al. 2010), detected oscillations of the magnetic flux density in small-scale magnetic elements in the quiet Sun. These oscillations, being in antiphase with area oscillations of the magnetic element, were consistent with intrinsic magnetic oscillations of the flux tube. The difficulty of mode identification was addressed by, e.g., Moreels & Van Doorsselaere (2013) and Moreels et al. (2013, 2015).

As mentioned earlier and underlined by Khomenko & Collados (2015), the detection of magnetic oscillations may suffer from cross-talk with other physical quantities. In the presence of a vertical gradient of the magnetic field, opacity effects may also play a significant role. In this regard, it is worth underlining that the phase analysis between different quantities can be important to verify the real nature of the detected oscillations in the solar atmosphere (see Moreels et al. 2015). This approach was already adopted by some authors (Balthasar 1999; Kupke et al. 2000) to discriminate between intrinsic magnetic fluctuations and cross-talks from other physical quantities such as temperature and density fluctuations associated with magneto-acoustic waves (Rüedi & Cally 2003). However, the phase lag analysis was limited to a single photospheric height. Extending the analysis to spectropolarimetric diagnostics acquired simultaneously at different heights in the solar atmosphere can provide new insight into the nature of these observed magnetic perturbations and, possibly, their propagation. This is the novel aspect and the main scope of this work.

2. Data Set and Methods

The data set used in this work was acquired on 2016 May 20 with the Interferometric BIdimensional Spectrometer (IBIS; Cavallini 2006; Reardon & Cavallini 2008) instrument at the National Solar Observatory Dunn Solar Telescope. The observations consist of a long time series (more than three hours) of full-Stokes high-spatial and temporal resolution spectropolarimetric scans (21 spectral points) of the Fe I 617.3 nm and Ca II 854.2 nm spectral lines of AR12546, one of the largest sunspots emergent onto the solar surface over the last 20 years. The spectral sampling is 20 mÅ and 60 mÅ for the Fe I 617.3 nm and Ca II 854.2 nm spectral lines, respectively. The cadence of the reduced data is 48 s, and the data set was acquired during stable seeing conditions for 184 min starting at 13: 39 UTC. At the beginning of the observation AR12546 was very close to the disk center (7° S, 2° W). The adaptive optics system (AO, Rimmele 2004) was locked and running on the center of the sunspot and the integration time was set to 80 ms. The theoretical diffraction-limited spatial resolution of the data was governed by the telescope aperture and the observed wavelengths, yielding 0.16 arcsec and 0.23 arcsec for the Fe 617.3 nm and Ca 854.2 nm spectral lines, respectively. During the acquisition period, the solar active region of interest (AR12546) was located at the disk center.

It is worth mentioning that the long duration of the data set, together with the fast acquisition cadence, is ideal for the study of oscillatory phenomena with periods ranging from 2 min (i.e., Nyquist sampling limit) showing the continuum intensity and the field strength, to ∼2 hr. Moreover, the availability of simultaneous observations at the photosphere and chromosphere allows us to search for signatures of propagation of magnetic field disturbances in circular polarization (CP) measurements, including an examination of the locations where this takes place.

In addition to the standard calibration procedures (i.e., flat-fielding, dark subtraction, and polarimetric calibrations), the images obtained were restored with MOMFBD (van Noort et al. 2005) techniques to limit the effects of the residual atmospheric aberrations left over by the AO system. In order to provide context over a larger field of view (FoV), in Figure 1 we show the continuum intensity, the field strength, and inclination maps derived from the *Hinode* SOT/SP near-simultaneous observations of the same region in the Fe I 630.1 nm and 630.2 nm spectral lines (Tsuneta et al. 2008). The maps are part of the SOT/SP level 2 data products (Lites & Ichimoto 2013), which are outputs from spectral line inversions using the MERLIN code,[9] and were downloaded from the HAO-CSAC (Community Spectro-polarimetric Analysis Center) data center.[10] Here, we note that this sunspot is very peculiar in both its size and magnetic field strength. Indeed, the field strength at the center of the umbra reaches values exceeding 4000 G. This is an uncommon magnetic field value for a sunspot (see, e.g., Rezaei et al. 2015 for a detailed analysis of the distribution of magnetic field strengths of sunspots). However, it is worth mentioning that Okamoto & Sakurai (2018) have reported field strengths in excess of 6000 G. In the same maps, the dotted–dashed box represents the IBIS FoV. Due to the large dimensions of the magnetic structure, the IBIS FoV nearly approximates the umbra diameter in the *x*-direction, while it includes part of the penumbra in the *y*-direction. In the same figure, we show an IBIS intensity image obtained in the core of the Fe 617.3 nm spectral line, the simultaneous chromospheric counterpart acquired in the core of the Ca II 854.2 nm spectral line, whose average height of formation is in the range 800–1000 km (Uitenbroek 2006), and the corresponding CP maps deduced from these IBIS observations. Also in this case, we note that the signal at the center of the umbra is very weak (∼100–200 data numbers). As previously described, the integration time of the IBIS instrument was set at 80 ms. This value was chosen so as to almost completely freeze the effects of the residual seeing, thus allowing the application of deconvolution techniques. For this reason, unfortunately, the integration time could not be extended to allow the increase of the photon flux at the center of the umbra.

In this study we measured the CP signal on a pixel-by-pixel basis by considering the amplitude of the Stokes-*V* profile:

$$\mathrm{CP} = \frac{|V_{\max}|}{I_{\mathrm{cont}}} \cdot \mathrm{sign}(V_{\max}), \quad (1)$$

where $V_{\max}$ is the maximum amplitude of the Stokes-*V* spectral profile, and I_{cont} the local continuum intensity. The choice of this particular definition of CP, instead of the more common integral of the Stokes-*V* profile, suits our goal to perform phase lag analyses between the photospheric and chromospheric channels. Indeed, the adopted definition results in the best spatial resolution when compared to other methods, since

[9] https://doi.org/10.5065/D6JH3J8D
[10] https://www2.hao.ucar.edu/csac

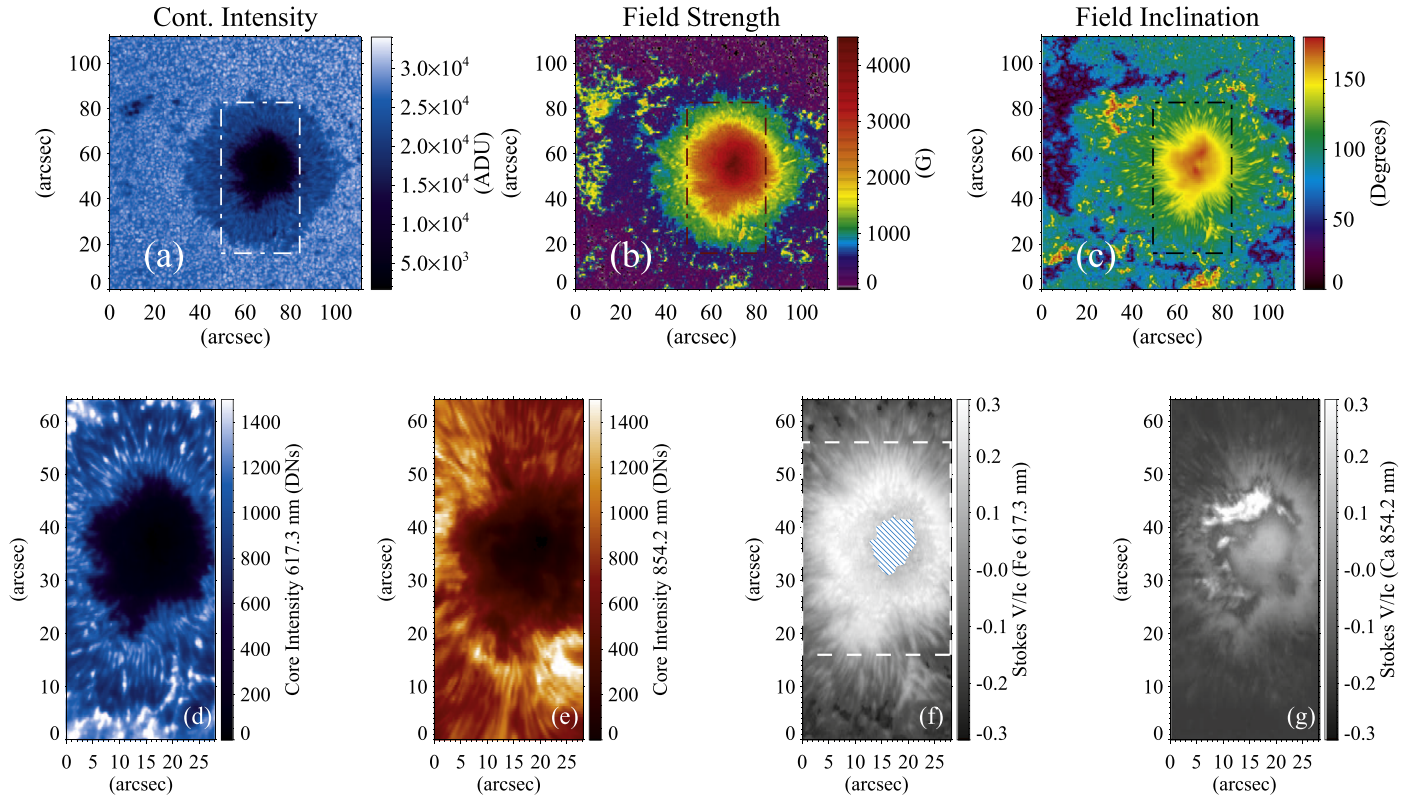

Figure 1. SOT/SP continuum intensity (panel a), magnetic field strength (panel b) and inclination (panel c) from *Hinode* level 2 data products. The dotted–dashed rectangular box represents the IBIS FoV. (Panels d and e): IBIS intensity images in the core of the Fe I 617.3 nm line and of the Ca II 854.2 nm line, respectively. (Panel f): CP map obtained from the IBIS Fe I 617.3 nm line measurements. The central region of the umbra that is affected by possible saturation effects and low photon flux is indicated as a hatched area. (Panel g): CP map derived from the IBIS Ca II 854.2 nm line data.

consecutive images during each scan of the corresponding spectral line are not summed up, preventing the smearing of small-scale details. Besides, the above definition also ensures the maximization of the spectral coherence between different layers.

The spectropolarimetric sensitivity of IBIS is very high and was estimated in Viticchié et al. (2010) as 10^{-3} times the continuum intensity level.

At the center of the studied sunspot, we observe a saturation of the polarization signals in the photosphere. This can be explained as a combination of different effects, namely, the low signal-to-noise ratio caused by the intrinsic photon flux at the center of the umbra, challenging the dynamic range of the detector (Centeno et al. 2014), and the saturation of the magnetic field sensitivity (see for instance Stenflo 2013), which occurs when Zeeman splitting becomes comparable with the line width and is typical of spectral lines with large Landé factors such as Fe I 617.3 nm ($g = 2.5$). For these reasons, the pixels at the center of the umbra are masked out in the maps. However, we note that this region is not included in any of the analyses of this work.

We studied the CP perturbations by applying a fast Fourier transform (FFT) coherence and phase analysis to CP signals at the two atmospheric heights sampled by the observations. In addition, we undertook phase correlation analyses between CP and intensity oscillations to attempt to identify a possible coupling between them.

In order to ensure the reliability of our results and their statistical significance, all the phase-lag diagrams reported in this work only include phase measurements that demonstrated coherence levels larger than 95%. Indeed, any phase estimate between signals with a small coherence should not be considered physically meaningful. We note that a coherence threshold of 95% corresponds to a very large confidence level, ensuring that accurate relationships (e.g., coupling) between the two different diagnostics are investigated.

It is worth noting that the time series of certain diagnostics in the solar atmosphere may be the result of the superposition of different oscillations and processes. There might be different modes present at the same time, and those showing a coupling (i.e., a particular phase lag) between, for example, different heights may have a much smaller amplitude compared to the dominant peak of the phase spectrum. In this regard, the coherence analysis can be seen as a filtering technique, which highlights the mere coupled components of two signals even if these components have a small amplitude compared to other dominant peaks of the power spectrum.

3. Results

3.1. CP–CP Phase

In Figure 2, we show the CP phase lag map (panel a) and its related coherence map (panel b) in the 3 mHz band (0.7 mHz bandwidth) as obtained from our FFT coherence analysis of the CP signals at the two atmospheric heights sampled by the Fe I 617.3 nm and Ca II 854.2 nm spectral lines. The map is obtained by averaging the phase values in this range. Our reasoning in choosing this frequency band will become apparent later in this section. Here, we note that the phase lag map displays a circular area of positive values of the phase

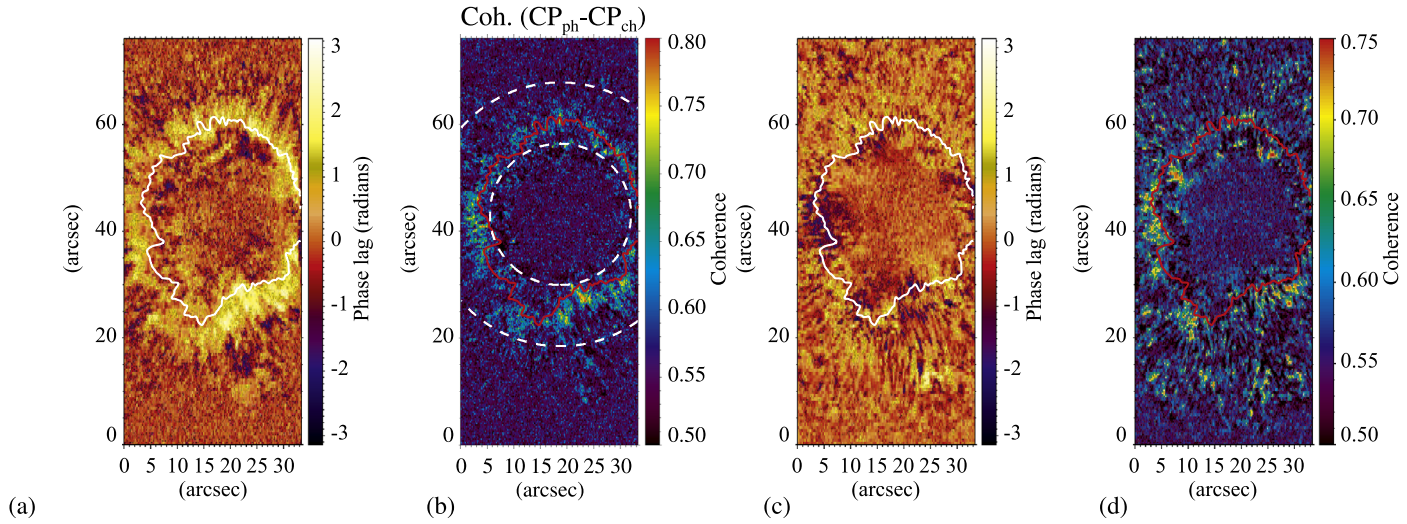

Figure 2. (a) Phase lag map of CP fluctuations at 3 mHz (with a bandwidth of 0.7 mHz) between the photosphere and chromosphere. (b) Coherence map at 3 mHz (with a bandwidth of 0.7 mHz) for the same CP disturbances. (c) Phase lag map at the same frequency band computed between CP fluctuations and core intensity fluctuations in the photosphere. (d) Coherence map corresponding to the phase map of panel (c). The continuous contours indicate the approximate position of the umbra–penumbra boundary as seen in the continuum intensity. The dashed lines highlight the region where the analysis was performed (see the text for more details). Note that the maps are obtained by averaging four spectral bins in Fourier space or, equivalently, 3.0 ± 0.7 mHz. For this reason, the average phase and coherence values might appear lower than they are at each frequency bin.

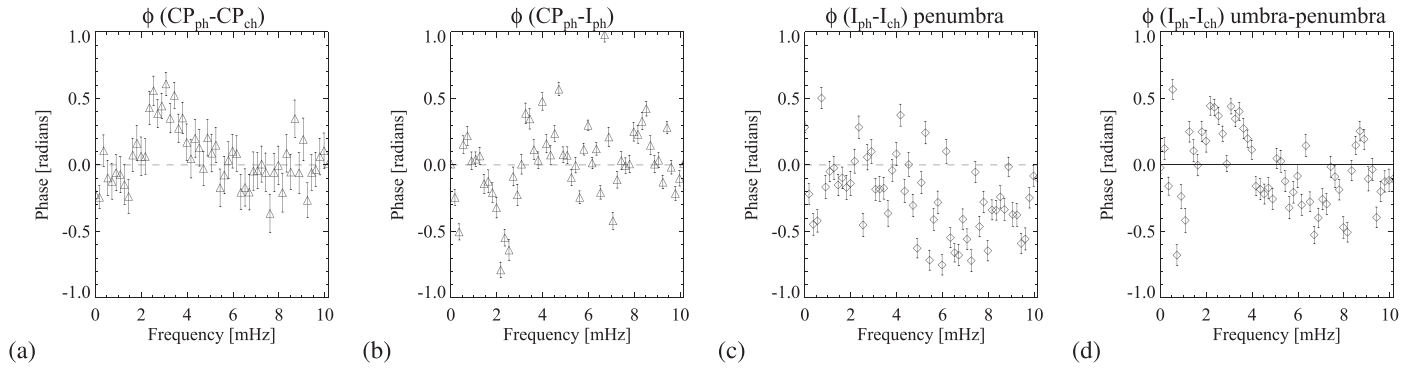

Figure 3. (a) Phase lag diagram between the CP signals in the photosphere and chromosphere computed in the annular region highlighted by the dashed lines in panel (b) of Figure 2. (b) CP–intensity phase diagram in the annular region of Figure 2 panel (b) estimated in the photosphere. All plots are obtained by considering only those phase values for which the coherence is larger than 95% in each frequency bin. (c) Phase lag diagram of intensity perturbations in the core of the Fe I 617.3 nm and Ca II 854.2 nm spectral lines in the penumbra outside the annular region of panel (b) Figure 2. (d) Phase lag diagram between intensity perturbations in the core of the Fe I 617.3 nm and Ca II 854.2 nm spectral lines. The diagram is obtained in the annular region highlighted by the dashed lines in panel (b) of Figure 2.

at the umbra–penumbra boundaries. In our sign convention a positive phase means that the photospheric signal is lagging behind the chromospheric counterpart (i.e., downward propagation of the perturbation). At the same location where a positive phase is observed (panel a), we also observe a large value of coherence (panel b). This fact ensures the reliability of the phase estimates themselves and can be regarded as strong evidence of coupling between the two CP signals at the two heights in the solar atmosphere. We remark that the phase lag is corrected for the time lag introduced by the instrumental sequential scanning of the spectral lines (i.e., the two spectral lines are scanned sequentially within 48 s). It is worth noting that any instrumental effect would not result in an annular spatial distribution of the propagating disturbances as shown in panel (a) of Figure 2.

The phase and coherence maps shown in this figure are the result of an average over four frequency bins or, equivalently, 3.0 ± 0.7 mHz. This means that the coherence can be lower than the maximum value found in a single frequency bin, due to the intrinsic dispersion of the phase measurements themselves. Despite this, the average coherence is quite large in the annular region, with frequency-averaged values exceeding 0.7. Indeed, as we will see, the maximum coherence at each frequency can be larger than this value and, in some cases, exceed 0.95.

In order to investigate further the phase spectrum between the photospheric and chromospheric signals, in panel (a) of Figure 3 we plot the phase spectrum obtained by considering only those pixels where the coherence is above 95% in the annular region highlighted by the dashed lines of Figure 2 (panel b) and in each frequency bin of the spectrum. It is worth noting that, in contrast to the phase maps of Figure 2 obtained by averaging the phase over four spectral bins, the phase diagrams here are obtained by over-plotting on the same graph only those phase measurements with a coherence larger than 0.95. For this reason, as was discussed previously, lower coherence values are found in the phase maps, albeit large enough (0.7–0.8) to be considered a robust confidence level.

The CP phase spectrum shows a distinct positive peak at 2.5–3 mHz, which is thus the frequency range considered to create the average maps shown in Figure 2.

3.2. *CP*–I *Phase*

In order to investigate whether the observed CP disturbances are associated with intensity oscillations, we also studied the relationship between the photospheric CP oscillations and the intensity fluctuations in the core of the Fe I 617.3 nm spectral line. The resulting phase and coherence maps at the same frequency band are shown in Figure 2, panels (c) and (d), respectively. We do not observe an annular region of positive phase values as clear as in the case of the CP–CP phase map of panel (a). Of course, here the phase relationship is determined at a single atmospheric height, with non-zero phase lags expected between particular MHD wave modes in CP–*I* measurements (Fujimura & Tsuneta 2009; Jess et al. 2015). However, the coherence map (panel d) does show large values at the umbra–penumbra boundaries and in the penumbra. This latter observation means that there exists a coupling between the CP and intensity perturbations (i.e., there is an intensity perturbation corresponding to a co-spatial CP perturbation).

The above coupling can be better seen in the phase diagram shown in panel (b) of Figure 3, derived from considering only those phase measurements with a coherence larger than 95%. This diagram is obtained in the annular region, including the umbra–penumbra boundaries, and highlighted by the dashed lines in Figure 2 (panel b). In this diagram we see that, although CP perturbations are accompanied by intensity perturbations, these are not necessarily in phase. Indeed, at the same frequency and spatial location where we observe propagating circular CP disturbances, we find negative phase values between CP–*I* fluctuations at photospheric heights. A negative phase in our sign convention means that intensity is lagging behind CP.

3.3. I–I *Phase*

In the previous section we found that, although there exists a coupling between CP and intensity, they are not in phase, and that the intensity perturbations are delayed with respect to the CP fluctuations. In order to complete this picture, we have studied the vertical propagation of intensity disturbances in the core of the two spectral lines sampled by IBIS. This was done in the penumbra (i.e., the region outside the dashed lines of Figure 2 panel (b)), and at the umbra–penumbra boundaries (i.e., the annular region shown in Figure 2 panel (b)). In particular, the penumbra was chosen as a reference and for comparison of the propagating regime observed in the umbra–penumbra boundaries. The results of this analysis are shown in panels (c) and (d) of Figure 3, where we plot the *I*–*I* phase diagram in the penumbra and at the umbra–penumbra boundary.

In the penumbra, we observe the upward propagation (negative phase) of the intensity oscillations for frequencies larger than 3–3.5 mHz. This is consistent with the presence of a cut-off frequency and upwardly propagating magneto-acoustic waves, which is consistent with the findings for running penumbral waves (Jess et al. 2013). However, in addition to this upward propagating regime for frequencies larger than 3–3.5 mHz, at the umbra–penumbra boundary we also observe a second positive-phase component at 2.5–3 mHz that was not detected in the penumbra (panel c of the same figure). Even in this case, the phase diagrams were obtained by only considering the phase measurements corresponding to a coherence larger than 95%.

4. Summary and Discussions

In this work, by taking advantage of a long-duration spectropolarimetric data set (more than three hours) sampling two different heights in the solar atmosphere, we have studied the propagation of CP disturbances in a large and symmetric sunspot, alongside their coupling with other physical quantities. The main findings of our work can be summarized by the following.

1. Downward propagating CP disturbances, at 2.5–3 mHz, are detected with a high confidence level at the umbra–penumbra boundary (see panel (a) and (b) of Figure 2).
2. At the same location where propagating CP fluctuations are identified, we also detected intensity oscillations that lag behind their corresponding CP perturbations (see panel (c) of Figure 3).

Several authors have reported oscillations of the Stokes profiles at the umbra–penumbra boundaries in sunspots, attributing them to temporal variations of the observed magnetic field (e.g., Rueedi et al. 1998; Balthasar 1999; Zhugzhda et al. 2000; Houston et al. 2018). Based on phase lag analyses between different observables restricted to a single height in the solar atmosphere, the same authors argued that these oscillations could be associated with real magnetic oscillations, excluding instrumental or opacity effects. However, this is a controversial opinion. Indeed, Settele et al. (2002) have underlined that several observational artifacts can introduce oscillations in the measurements of the magnetic field vector, e.g., seeing effects, instrumental cross-talk from velocity, and opacity effects.

In our study, artifacts from instrumental cross-talk from velocity can be ruled out by the phase delay measured between the magnetic perturbations and the velocity itself, displayed in Figure 4. We note that the frequency, spatial coherence, and vertical propagation of the disturbances are all aspects that make seeing effects unlikely to contribute to the obtained results. However, as already stressed in Bellot Rubio et al. (2000), a definitive interpretation of the oscillations in the magnetic field would only be possible through the study of the fluctuations of atmospheric diagnostics and their stratification in terms of geometrical heights. Unfortunately, this is not a trivial task, as it requires the identification of a reference height, which is also subject to opacity effects. However, by comparing a theoretical model to observations, Khomenko et al. (2003) have argued that the observed fluctuations of the magnetic field are the result of a mixture of intrinsic magnetic oscillations, though rather small (a few G), and time-varying opacity effects due to magneto-acoustic waves. In particular, they found that toward the edges of the umbra it is impossible to reproduce the observations without including the intrinsic oscillations of the magnetic field that characterize the fast MHD mode, something that has recently been further quantified by Grant et al. (2018). Once again we stress that, in contrast to the power spectrum where a small coherent signal might be hidden in other dominant components, the phase lag and coherence analysis acts as a robust "de-noising" technique, highlighting small-amplitude, yet coherent (between different layers)

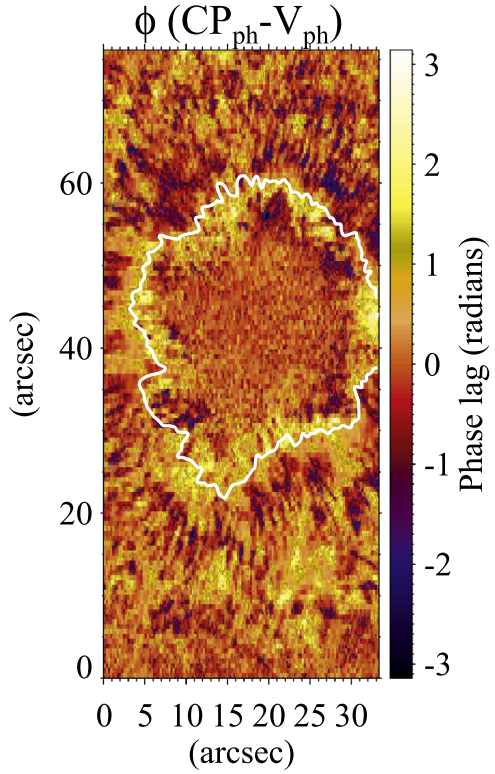

Figure 4. Phase lag map between CP and LoS velocity measured in the photospheric Fe I 617.3 nm data.

signals. In this regard, our techniques may identify only the coherent part of downwardly propagating CP perturbations, regardless of their amplitudes.

Our analysis also reveals coupled intensity perturbations lagging behind their corresponding CP fluctuations. This is in contrast with Balthasar (1999), who found no statistically significant relationship between intensity and magnetic field variations. The coherence between the two signals in their case was in fact below 0.5, therefore it was too small to draw conclusions on a possible relationship between the two quantities. However, we note that a lower coherence value may have resulted, in their case, from the lower quality of the data set employed by the authors with respect to the one studied here. Indeed, no AO was available, and this resulted in larger dynamic optical aberrations that may have reduced the coherence between the different quantities investigated. In this sense, our results regarding the coupling of CP and intensity oscillations are not in contrast to those obtained by Balthasar (1999), but simply underline the necessity of very good seeing conditions for accurate phase lag analyses.

In the case of opacity effects, where the magnetic field fluctuations are a consequence of the vertical magnetic field gradient (i.e., dB/dz), we expect the intensity oscillations to be out of phase with the CP fluctuations. This is not the case for our observations, thus the presence of genuine magnetic fluctuations appears to be a reasonable conclusion.

In this regard it is worth recalling that Joshi & de la Cruz Rodríguez (2018) have intensely investigated magnetic oscillations in the umbra and penumbra of a sunspot through non-local thermal equilibrium spectropolarimetric inversions at chromospheric heights, and found magnetic field variations that are not in agreement with opacity effects.

We note that the phase diagram of intensity oscillations between two layers shows the coexistence of two modes at the umbra–penumbra boundary: upward propagating waves for frequencies above the cut-off, and downward propagating oscillations at 2.5–3 mHz. The latter are also accompanied by downward propagating CP oscillations.

In an attempt to explain the presence of magnetic oscillations at the umbra–penumbra boundary, Zhugzhda et al. (1999) have shown theoretically that these oscillations can be ascribed to either slow surface or body modes, although the first option was soon ruled out since it is expected that a surface mode would appear in a thin layer with an estimated width of ∼100 km. In our case, the width of the region showing the presence of propagating CP oscillations is of the order of 10 arcsec, or equivalently 7500 km. Nevertheless, the absence of propagating disturbances in the umbra of the sunspot seems to agree with the surface wave scenario. Here, we note that the detection of downward propagating surface disturbances in the sunspot is independent of the possible contamination of opacity effects on the CP signals. Indeed, as mentioned previously, it was demonstrated that these opacity effects would be the signature of magneto-acoustic perturbations in any case. Recent work by Keys et al. (2018) provided a framework for directly detecting surface and body modes in pores, which are simpler structures in comparison to sunspots. The inclination of penumbral fields means that these techniques are more complicated to apply to our data to verify our belief that these oscillations are surface modes. Although it is outside the scope of this current study, in future work we will look to adapt these techniques to work with sunspots and to determine conclusively if these oscillations are surface modes.

This research has received funding from the European Union's Horizon 2020 research and innovation program under the grant agreements No. 739500 (project PRE-EST) and No. 824135 (project SOLARNET) and partly supported by the "Progetti di ricerca INAF di Rilevante Interesse Nazionale" (PRIN-INAF) 2014 and PRIN-MIUR 2012 (prot. 2012P2HRCR) entitled "Il sole attivo ed i suoi effetti sul clima dello spazio e della terra" grants, funded by the Italian National Institute for Astrophysics (INAF) and Ministry of Education, Universities and Research (MIUR), respectively. The National Solar Observatory is operated by the Association of Universities for Research in Astronomy under a cooperative agreement with the National Science Foundation. IBIS has been built by the INAF-Arcetri Astrophysical Observatory, with the support of the Department of Physics and Astronomy of the University of Florence, and the Department of Physics of the University of Rome–Tor Vergata. It is operated and supported by INAF in collaboration with the US National Solar Observatory. R.E. thanks the Science and Technology Facilities Council (STFC, grant numbers ST/M000826/1, ST/L006316/1) for the support to conduct this research. S.J. acknowledges support from the European Research Council (ERC) under the European Union's Horizon 2020 research and innovation program (grant agreement No. 682462) and from the Research Council of Norway through its Centres of Excellence scheme, project number 262622. D.B.J. would like to thank the STFC for the award of an Ernest Rutherford Fellowship, in addition to a dedicated standard grant which allowed this project to be undertaken. D.B.J. also wishes to thank Invest NI and Randox Laboratories Ltd. for the award of a Research & Development Grant (059RDEN-1). P.H.K. would

like to thank the Leverhulme Trust for the award of an early career fellowship. *Hinode* is a Japanese mission developed and launched by ISAS/JAXA, collaborating with NAOJ as a domestic partner, and NASA and UKSA as international partners. Scientific operation of the *Hinode* mission is conducted by the *Hinode* science team organized at ISAS/JAXA. This team mainly consists of scientists from institutes in the partner countries. Support for the post-launch operation is provided by JAXA and NAOJ (Japan), UKSA (U.K.), NASA, ESA, and NSC (Norway).

ORCID iDs

M. Stangalini https://orcid.org/0000-0002-5365-7546
S. Jafarzadeh https://orcid.org/0000-0002-7711-5397
I. Ermolli https://orcid.org/0000-0003-2596-9523
R. Erdélyi https://orcid.org/0000-0003-3439-4127
D. B. Jess https://orcid.org/0000-0002-9155-8039
P. H. Keys https://orcid.org/0000-0001-8556-470X
M. Murabito https://orcid.org/0000-0002-0144-2252
F. Berrilli https://orcid.org/0000-0002-2276-3733

References

Allcock, M., & Erdélyi, R. 2017, SoPh, 292, 35
Balthasar, H. 1999, SoPh, 187, 389
Bellot Rubio, L. R., Collados, M., Ruiz Cobo, B., & Rodríguez Hidalgo, I. 2000, ApJ, 534, 989
Bloomfield, D. S., Lagg, A., & Solanki, S. K. 2007, ApJ, 671, 1005
Bogdan, T. J. 2000, SoPh, 192, 373
Braun, D. C., Duvall, T. L., Jr., Labonte, B. J., et al. 1992, ApJL, 391, L113
Cally, P. S., Bogdan, T. J., & Zweibel, E. G. 1994, ApJ, 437, 505
Cavallini, F. 2006, SoPh, 236, 415
Centeno, R., Collados, M., & Trujillo Bueno, J. 2006, ApJ, 640, 1153
Centeno, R., Schou, J., Hayashi, K., et al. 2014, SoPh, 289, 3531
Chorley, N., Hnat, B., Nakariakov, V. M., Inglis, A. R., & Bakunina, I. A. 2010, A&A, 513, A27
Crouch, A. D., & Cally, P. S. 2005, SoPh, 227, 1
CSAC 2016, Hinode SOT/SP Data
Edwin, P., & Roberts, B. 1983, SoPh, 88, 179
Fedun, V., Shelyag, S., & Erdélyi, R. 2011, ApJ, 727, 17
Felipe, T., Khomenko, E., & Collados, M. 2010, ApJ, 719, 357
Felipe, T., Khomenko, E., & Collados, M. 2011, ApJ, 735, 65
Freij, N., Scullion, E. M., Nelson, C. J., et al. 2014, ApJ, 791, 61
Fujimura, D., & Tsuneta, S. 2009, ApJ, 702, 1443
Grant, S. D. T., Jess, D. B., Moreels, M. G., et al. 2015, ApJ, 806, 132
Grant, S. D. T., Jess, D. B., Zaqarashvili, T. V., et al. 2018, NatPh, 14, 480
Horn, T., Staude, J., & Landgraf, V. 1997, SoPh, 172, 69
Houston, S. J., Jess, D. B., Asensio Ramos, A., et al. 2018, ApJ, 860, 28
Jafarzadeh, S., Solanki, S. K., Stangalini, M., et al. 2017, ApJS, 229, 10
Jefferies, S. M., McIntosh, S. W., Armstrong, J. D., et al. 2006, ApJL, 648, L151
Jess, D. B., Mathioudakis, M., Erdélyi, R., et al. 2009, Sci, 323, 1582
Jess, D. B., Morton, R. J., Verth, G., et al. 2015, SSRv, 190, 103
Jess, D. B., Reznikova, V. E., Van Doorsselaere, T., Keys, P. H., & Mackay, D. H. 2013, ApJ, 779, 168
Jess, D. B., Van Doorsselaere, T., Verth, G., et al. 2017, ApJ, 842, 59
Joshi, J., & de la Cruz Rodríguez, J. 2018, arXiv:1803.01737
Keys, P. H., Morton, R. J., Jess, D. B., et al. 2018, ApJ, 857, 28
Khomenko, E., & Collados, M. 2015, LRSP, 12, 6
Khomenko, E., Collados, M., & Felipe, T. 2008, SoPh, 251, 589
Khomenko, E. V., Collados, M., & Bellot Rubio, L. R. 2003, ApJ, 588, 606
Krishna Prasad, S., Jess, D. B., Van Doorsselaere, T., et al. 2017, ApJ, 847, 5
Kupke, R., Labonte, B. J., & Mickey, D. L. 2000, SoPh, 191, 97
Lites, B. W., & Ichimoto, K. 2013, SoPh, 283, 601
Lites, B. W., Thomas, J. H., Bogdan, T. J., & Cally, P. S. 1998, ApJ, 497, 464
Löhner-Böttcher, J. 2016, PhD thesis, Universität Freiburg im Breisgau
Martínez González, M. J., Asensio Ramos, A., Manso Sainz, R., et al. 2011, ApJL, 730, L37
Mathioudakis, M., Jess, D. B., & Erdélyi, R. 2013, SSRv, 175, 1
McIntosh, S. W., & Jefferies, S. M. 2006, ApJL, 647, L77
Moreels, M. G., Freij, N., Erdélyi, R., Van Doorsselaere, T., & Verth, G. 2015, A&A, 579, A73
Moreels, M. G., Goossens, M., & Van Doorsselaere, T. 2013, A&A, 555, A75
Moreels, M. G., & Van Doorsselaere, T. 2013, A&A, 551, A137
Moretti, P. F., Jefferies, S. M., Armstrong, J. D., & Mc Intosh, S. W. 2007, A&A, 471, 961
Morton, R. J., Erdélyi, R., Jess, D. B., & Mathioudakis, M. 2011, ApJL, 729, L18
Morton, R. J., Verth, G., Jess, D. B., et al. 2012, NatCo, 3, 1315
Mumford, S. J., & Erdélyi, R. 2015, MNRAS, 449, 1679
Mumford, S. J., Fedun, V., & Erdélyi, R. 2015, ApJ, 799, 6
Okamoto, T. J., & Sakurai, T. 2018, ApJL, 852, L16
Pintér, B., & Erdélyi, R. 2018, AdSpR, 61, 759
Reardon, K. P., & Cavallini, F. 2008, A&A, 481, 897
Rezaei, R., Beck, C., Lagg, A., et al. 2015, A&A, 578, A43
Rimmele, T. R. 2004, Proc. SPIE, 5490, 34
Roberts, B. 1983, Sol. Phys., 87, 77
Rüedi, I., & Cally, P. S. 2003, A&A, 410, 1023
Rüedi, I., Solanki, S. K., Bogdan, T., & Cally, P. 1999, in Polarization, Astrophysics and Space Science Library, Vol. 243, ed. K. N. Nagendra & J. O. Stenflo (Dordrecht: Kluwer), 337
Rueedi, I., Solanki, S. K., Stenflo, J. O., Tarbell, T., & Scherrer, P. H. 1998, A&A, 335, L97
Settele, A., Sigwarth, M., & Muglach, K. 2002, A&A, 392, 1095
Solanki, S. K., Barthol, P., Danilovic, S., et al. 2010, ApJL, 723, L127
Stangalini, M., Del Moro, D., Berrilli, F., & Jefferies, S. M. 2011, A&A, 1, 1
Stangalini, M., Giannattasio, F., Del Moro, D., & Berrilli, F. 2012, A&A, 539, L4
Staude, J. 2002, AN, 323, 317
Stenflo, J. O. 2013, A&Ar, 21, 66
Tsuneta, S., Ichimoto, K., Katsukawa, Y., et al. 2008, SoPh, 249, 167
Uitenbroek, H. 2006, in ASP Conf. Ser. 354, Solar MHD Theory and Observations: A High Spatial Resolution Perspective, ed. J. Leibacher, R. F. Stein, & H. Uitenbroek (San Francisco, CA: ASP), 313
van Noort, M., Rouppe van der Voort, L., & Löfdahl, M. G. 2005, SoPh, 228, 191
Vigeesh, G., Fedun, V., Hasan, S. S., & Erdélyi, R. 2012, ApJ, 755, 18
Viticchié, B., Del Moro, D., Criscuoli, S., & Berrilli, F. 2010, ApJ, 723, 787
Zhugzhda, Y., Balthasar, H., & Staude, J. 1999, in ESA , Magnetic Fields and Solar Processes, Vol. 448 ed. A. Wilson et al. (Noordwijk: ESA), 417
Zhugzhda, Y. D., Balthasar, H., & Staude, J. 2000, A&A, 355, 347
Zsámberger, N. K., Allcock, M., & Erdélyi, R. 2018, ApJ, 853, 136